

LETTER TO THE EDITOR

The column density towards LMC X-1

Manfred Hanke¹, Jörn Wilms¹, Michael A. Nowak², Laura Barragán¹, and Norbert S. Schulz²

¹ Dr. Karl Remeis-Observatory & ECAP, University of Erlangen-Nuremberg, Sternwartstr. 7, 96049 Bamberg, Germany
e-mail: Manfred.Hanke@sternwarte.uni-erlangen.de

² MIT Kavli Institute for Astrophysics and Space Research, NE80-6077, 77 Mass. Ave., Cambridge, MA 02139, USA

Received: 3 November 2009 / Accepted: 17 December 2009

ABSTRACT

We measure the neutral absorption towards the black hole X-ray binary system LMC X-1 from six archival soft X-ray spectra obtained with the gratings and/or CCD detectors on *Chandra*, *XMM-Newton*, and *Swift*. Four spectral models for the soft continuum have been investigated. While the `powerlaw` model may overestimate N_{H} considerably, the others give consistent results. Taking the lower metallicity of the Large Magellanic Cloud into account, we find equivalent hydrogen column densities of $N_{\text{H}}=(1.0\text{--}1.3)\times 10^{22}\text{ cm}^{-2}$, with a systematic dependence on the orbital phase. This variation of the neutral absorption can nearly explain the orbital modulation of the soft X-ray flux recently detected with the All Sky Monitor (ASM) on the *Rossi X-ray Timing Explorer (RXTE)*.

Key words. X-rays: individuals (LMC X-1) – X-rays: binaries – X-rays: ISM – Galaxies: abundances

1. Introduction

The extragalactic X-ray sources in the Large Magellanic Cloud (LMC), our ≈ 48 kpc distant neighbor galaxy, were discovered in the late 1960s (Mark et al., 1969; Price et al., 1971). Due to the high density of stars, their optical identifications were uncertain for a long time. The X-ray binary system (XRB) LMC X-1 is located $\approx 0^{\circ}5$ south-southeast of the 30 Doradus star-formation region, in the NGC 2078 (LMC N159F) nebula. Pakull (1980), Hutchings et al. (1983, 1987), and Cowley et al. (1995) were able to identify the counterpart of LMC X-1 with a $m_V=14^m5$ O7/8 giant (Hutchings et al., 1983; Negueruela & Coe, 2002). This has allowed the placement of strong dynamical constraints on the compact object's mass. Orosz et al. (2009) recently have used optical spectra of this star – labeled as ‘star #32’ by Cowley et al. (1978) and also often called Pakull's star – to confirm the black hole (BH) candidacy of LMC X-1. They derive an orbital period of 3.909 d which is consistent with the modulation of the soft X-ray flux of LMC X-1 (Levine & Corbet, 2006). Deriving an extinction of $A_V = 2.28 \pm 0.06$ – much more than previously assumed – from the $V-K$ color excess, Orosz et al. (2009) infer a BH mass of $10.9 \pm 1.6 M_{\odot}$.

The persistent XRB LMC X-1 is the only dynamically confirmed BH candidate which so far has only been found in the high/soft (thermal dominant) X-ray spectral state. That is, its X-ray spectrum can be described by a multi-temperature disk blackbody component plus a weak soft ($\Gamma \gg 2$) power law component (Ebisawa et al., 1989; Schlegel et al., 1994; Wilms et al., 2001; Nowak et al., 2001; Haardt et al., 2001; Cui et al., 2002; Yao et al., 2005). In comparison, LMC X-3 usually shows a similarly soft X-ray spectrum, but also (partial) transitions to the low/hard state (Wilms et al., 2001; Smith et al., 2007), while Cyg X-1 regularly transits between the low/hard and a soft-intermediate state and never reaches the thermal dominant state (Wilms et al., 2006). LMC X-1 is there-

fore an ideal target to measure the BH spin parameter a_* from the soft X-ray continuum produced by the relativistic accretion disk. Gierliński et al. (2001) constrained a_* to be less than 0.998 from a 24 ks 0.7–10 keV ASCA-SIS spectrum. Gou et al. (2009) have recently reported $a_* = 0.90^{+0.04}_{-0.09}$ from 18 selected RXTE-PCA spectra with exposures between 5–11 ks and covering 2.5–20 keV. The latter authors fix the column density for the photoelectric absorption to $N_{\text{H}} = 4.6 \times 10^{21}\text{ cm}^{-2}$ as reported by Cui et al. (2002) based on low statistics data.

An appropriate description of the absorption is, however, indispensable for modeling the soft X-ray continuum and likewise for modeling the visual extinction, and thus the derivation of the system parameters from the dereddened optical spectrum of the companion star. In this Letter, we therefore aim to accurately describe the column density towards LMC X-1. We describe the data in §2 and present the methods and our analysis in §3. We summarize and discuss our results in §4.

2. Observations and Data Reduction

We study the spectra from all six recent observations with instruments providing soft X-ray spectra (Table 1).

The *Chandra* observation C1 was performed using the HETGS (Canizares et al., 2005) and with the detector CCDs operated in timed exposure mode. The \pm first order HEG and MEG spectra as well as the corresponding response matrices were taken from the *Chandra* Transmission Grating Catalog archive TGCat¹.

All instruments of *XMM-Newton* (Jansen et al., 2001) were active during the first (shorter) *XMM* observation X1. The EPIC-pn camera (Strüder et al., 2001) was operated in timing mode. Its data are therefore not affected by photon pile-up (Wilms et al., 2003). The same is true for data from the Reflection Grating Spectrometers (RGS; den Herder

¹ See <http://tgcath.mit.edu>.

Table 1. Log of recent soft X-ray observations of LMC X-1 with good S/N (Instruments not considered here are in parenthesis.)

Obs.	Start Date	Start Date (MJD)	Exposure (ks)	$\phi_{\text{orb}}^{(T3)\dagger}$	$\phi_{\text{orb}}^{(F9)\ddagger}$	Satellite	ObsID	Instruments
C1	2000-01-16	51559.2	19	0.45–0.51	0.50–0.56	<i>Chandra</i>	93	HETGS
X1	2000-10-21	51838.7	5–7	0.94–0.96	0.98–0.01	<i>XMM</i>	0112900101	PN, RGS 1+2, (MOS 1+2)
X2	2002-09-26	52543.2	35	0.17–0.28	0.21–0.32	<i>XMM</i>	0023940401	RGS 1+2, (MOS 1+2)
S1	2007-10-31	54404.7	2.4	0.37–0.42	0.37–0.43	<i>Swift</i>	00037079001	(BAT), XRT/PC, (UVOT)
S2	2007-12-06	54440.4	9.8	0.49–0.61	0.50–0.62	<i>Swift</i>	00037079002	(BAT), XRT/WT, (UVOT)
S3	2007-12-10	54444.1	4.4	0.43–0.50	0.43–0.50	<i>Swift</i>	00037079003	(BAT), XRT/WT, (UVOT)

[†] orbital phase calculated from the ephemeris of Orosz et al. (2009, Table 3): $T_0 = \text{MJD } 53390.8436$, $P = 3.90917 \text{ d}$

[‡] orbital phase calculated from the ephemeris of Orosz et al. (2009, Fig. 9): $T_0 = \text{MJD } 53390.75174$, $P = 3.9094 \text{ d}$

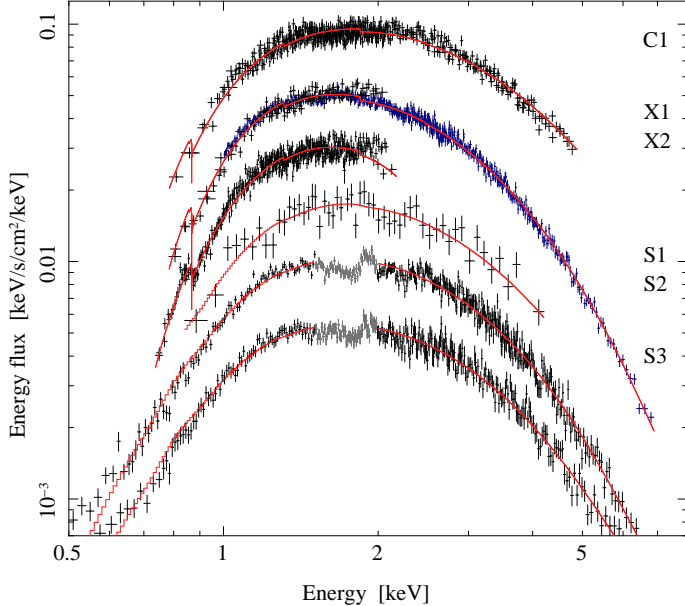


Fig. 1. Flux-corrected spectra of LMC X-1 from the six observations, shifted in flux according to the labels with respect to C1 for visual clarity. The gray data have been ignored because of calibration issues. Note that the models shown here for illustrative purposes are also broadened by the instrumental response.

et al., 2001) due to their dispersion of the photons, but not for data from the MOS cameras (Turner et al., 2001), which were operated in full frame imaging mode. For this reason, we only use the EPIC-pn spectrum and the first and second order spectra of RGS 1 and 2. For the second (longer) *XMM* observation X2, however, no pn-data are available. The data were reduced with the Science Analysis Software, *xmmsas*, v. 7.1, following standard procedures, i.e., applying the SAS tasks *epchain*, *emchain*, *rgsproc*, *evselect*, *rmfgen* and *arfgen* to produce spectra and response matrices.

Swift's X-ray telescope (XRT; Burrows et al., 2005) was operated in photon counting (PC) mode during the first *Swift* observation S1, which resulted in pile-up. For S2 and S3, the windowed timing (WT) mode was used. After reprocessing the data to apply the newest calibration, spectra were extracted using standard *FTOOLS*, handled via *xselect*. For the PC mode observation S1, we extract an annulus to exclude the region affected by pile-up, yielding a low quality spectrum only. Ancillary response files were created with *xrtmkarf*, and suitable response files for each observation were obtained from the CALDB. The WT mode spectra are not as well calibrated as the PC mode one around the Si edge (Fig. 1); we therefore exclude their 1.5–2 keV data.

Table 2. Comparison of elemental abundances (by number) in the Galactic ISM and in the LMC as $\epsilon(X) = 12 + \log_{10}(X/H)$

X	$\epsilon_{\text{gal}}(X)^{(1)}$	$\epsilon_{\text{LMC}}(X)$	$10^{\Delta\epsilon(X)}$
He	10.99	10.93 ⁽⁵⁾	0.87
C	8.38	8.03 ⁽²⁾	0.45
N	7.88	7.01 ⁽²⁾	0.13
O	8.69	8.38 ⁽²⁾	0.49
Ne	7.94	7.6 ⁽⁴⁾	0.46
Mg	7.40	7.12 ⁽²⁾	0.53
Si	7.27	7.21 ⁽²⁾	0.87
S	7.09	6.7 ⁽⁴⁾	0.41
Ar	6.41	6.2 ⁽⁴⁾	0.62
Fe	7.43	7.2 ⁽³⁾	0.59

References.

- (1) Wilms et al. (2000) or using `xspec_abund("wilm")`; in *ISIS*.
- (2) Przybilla (priv. comm.): average of 7 B-stars in the LMC (see also Korn et al., 2002, 2005).
- (3) Przybilla (priv. comm.): 1 star in the LMC (see also Przybilla et al., 2008).
- (4) Garnett (1999): HII regions in the LMC.
- (5) Dufour (1984).

Note.

The last column is the LMC abundance relative to the Galactic abundance, which is a parameter of the `tbvarabs` absorption model (Wilms et al., 2000, 2009, in prep.). For all other elements (which hardly contribute to the absorption in the soft X-ray band), the average value $10^{\Delta\epsilon(X)} = 0.5$ is assumed.

All spectral analysis was performed with the Interactive Spectral Interpretation System (*ISIS*; Houck & Denicola, 2000; Noble et al., 2006; Noble & Nowak, 2008)².

3. Analysis

An overview of previous N_{H} measurements for LMC X-1 is given by Orosz et al. (2009, Table 2). We caution, however, that only <12% of the hydrogen column density towards the LMC, $N_{\text{H}} = 4 \times 10^{21} \text{ cm}^{-2}$ (measured in the LAB 21 cm survey; Kalberla et al., 2005; Bajaja et al., 2005), is of Galactic origin,³ while the largest part is detected at $v_{\text{LSR}} = 200\text{--}300 \text{ km s}^{-1}$ and thus is likely local to the LMC (Richter et al., 1987). As the absorption in the 0.5–10 keV band is mostly caused by metals (Wilms et al., 2000), and the LMC has a much lower metallicity than our Galaxy, we compile both abundance sets in Table 2. The LMC abundances are henceforth used throughout our analysis.

² See <http://space.mit.edu/cxc/isis/>.

³ See http://www.astro.uni-bonn.de/~webaiub/english/tools_labsearch.php?alpha=05+39+38.7&beta=-69+44+36.

Table 3. Column density in units of 10^{22} cm^{-2} for the six observations and the sine fit, obtained with different continuum models

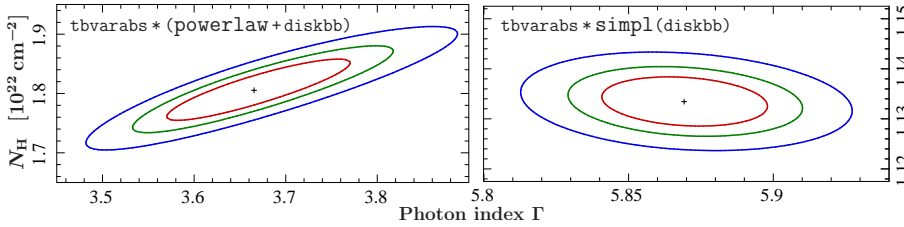
Observation or Fit	X2	S1	S3	C1	S2	X1	Sine Fit
$\phi_{\text{orb}}^{(\text{T3})}$	0.17–0.28	0.37–0.42	0.43–0.50	0.45–0.51	0.49–0.61	0.94–0.96	full orbit
diskbb+powerlaw*	$(2.00^{+0.17}_{-0.19})^*$	$(1.2^{+0.5}_{-0.2})^*$	$0.96^{+0.03}_{-0.02}$	$(1.25^{+0.04}_{-0.01})^*$	1.031 ± 0.017	$(1.81^{+0.06}_{-0.05})^*$	$(1.43 \pm 0.43)^*$
eqpair	1.279 ± 0.005	$1.17^{+0.15}_{-0.10}$	1.02 ± 0.02	$1.065^{+0.000}_{-0.019}$	1.088 ± 0.017	$1.191^{+0.006}_{-0.007}$	1.15 ± 0.15
simpl(kerrbb)	1.278 ± 0.005	$1.17^{+0.11}_{-0.10}$	$1.01^{+0.03}_{-0.02}$	$1.085^{+0.018}_{-0.016}$	1.088 ± 0.017	$1.187^{+0.014}_{-0.012}$	1.15 ± 0.14
simpl(diskbb)	$1.288 \pm 0.016^\dagger$	$1.14^{+0.15}_{-0.11}$	0.97 ± 0.02	$1.009^{+0.018}_{-0.017}$	1.038 ± 0.017	$1.133^{+0.005}_{-0.004}$	1.10 ± 0.18

Notes.

Quoted errors are statistical uncertainties at the 90% confidence level for the observations, but semi-amplitudes for the sine fits.

* Note that the **diskbb+powerlaw** model overestimates N_{H} the more, the more the **powerlaw** contributes at low energies, see text.

† As the lack of data above 2 keV did not allow to constrain the power law with the **simpl** model, we here used **diskbb** only.

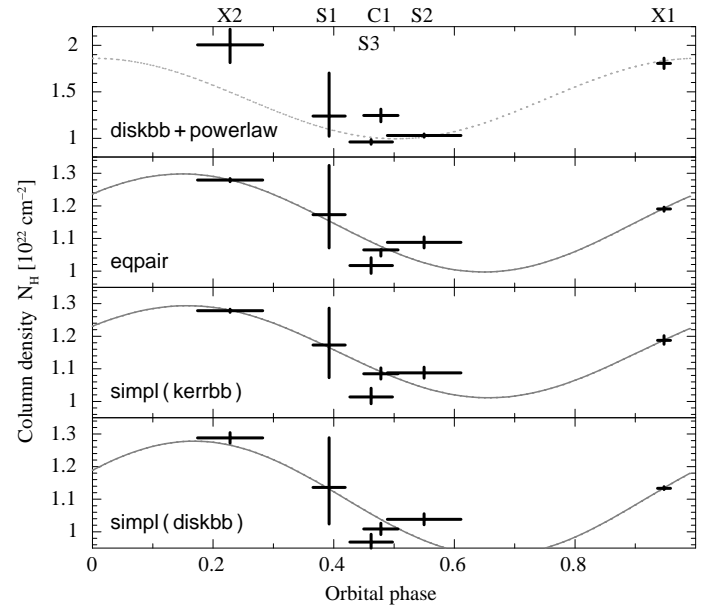
**Fig. 2.** Correlation of the column density N_{H} and the photon index Γ , derived with the **powerlaw** model (left) and the **simpl** model (right) for observation X1. The contours show the 68%, 90% and 99% confidence regions for two parameters of interest (i.e., $\Delta\chi^2 = 2.30, 4.61, \text{ and } 9.21$).

As for all previous observations (see § 1), the X-ray spectra of LMC X-1 investigated here are very soft (see Fig. 1), but a hard (albeit very steep) component in addition to a thermal one is nonetheless needed to describe the data, except for S2 and S3. The **powerlaw** model, however, becomes unphysically strong at low energies (e.g., Shrader & Titarchuk, 1998; Done et al., 2002). A steep photon index $\Gamma \gg 2$ (e.g., $\Gamma = 3.7 \pm 0.1$ as measured for X1, which has the best high-energy coverage due to the EPIC-pn spectrum) is compensated in spectral fits by an incorrectly strong absorption (e.g., Yao et al., 2005; Suchy et al., 2008; Gou et al., 2009). In contrast, the empirical convolution model **simpl** (Steiner et al., 2009) has an intrinsic *low-energy* cut-off when convolving an input spectrum modeled by, e.g., **diskbb** or **kerrbb**.⁴ Figure 2 shows that the (well known) correlation between N_{H} and Γ vanishes when **simpl** is used instead of **powerlaw**. Although an even steeper photon index was found using **simpl**, the value of N_{H} is smaller and is more narrowly constrained.

As the derived absorption might depend on the shape of the continuum, we investigate different models, namely empirical ones – such as **diskbb+powerlaw**, **simpl(diskbb)**, and **simpl(kerrbb)** (Li et al., 2005) – as well as the physical Comptonization model **eqpair** (Coppi, 2000).⁵ Here, these models typically describe the data equally well. In all fits, the disk has a temperature between 0.65 and 1.1 keV. The other parameters, too, are similar to previously obtained values. Table 3 and Fig. 3 show our results for the column density (assuming the LMC abundances given in Table 2) as a function of orbital phase ϕ_{orb} for each of the six observations and all four aforementioned continuum models. In all cases where a steep power law substantially contributes to the model, the **diskbb+powerlaw** model gives a much higher N_{H} than the other models, due to the systematic error of the **powerlaw** model. We there-

⁴ Note that – as a convolution model that relies upon a spectral model outside of the energy range spanned by the noticed data – **simpl** must be evaluated on a suitably extended grid.

⁵ For X1, the N_{H} derived with **diskbb+compTT** (Titarchuk, 1994) is also consistent with the one from, e.g., **simpl(diskbb)**.

**Fig. 3.** N_{H} as a function of orbital phase $\phi_{\text{orb}}^{(\text{T3})}$ (see Table 1) using various continuum models. Note the different scale for the **diskbb+powerlaw** model, which may predict an unreliably large N_{H} (see text). The gray lines fit the results with sine curves.

fore ignore these values. The other models, however, are quite consistent with one another; their agreement on N_{H} is within $< 8 \times 10^{20} \text{ cm}^{-2}$, which is therefore an upper limit of the systematic error due to the choice of the continuum. Using the LMC abundances (Table 2), we find column densities in the range of $(1.0\text{--}1.3) \times 10^{22} \text{ cm}^{-2}$.

We detect a modulation of N_{H} with orbital phase: the observations X1 and X2 close to $\phi_{\text{orb}} \approx 0$, when the BH is behind the donor star, require a systematically higher N_{H} than S3, C1, and S2 close to $\phi_{\text{orb}} \approx 0.5$. In order to quantify this modulation by its mean and amplitude (Table 3), we fit sine curves to the six measurements for each continuum model (see Fig. 3), being aware that they do not describe the data very well and also predict the strongest absorption at $\phi_{\text{orb}} = 0.15\text{--}0.17$, which is not expected.

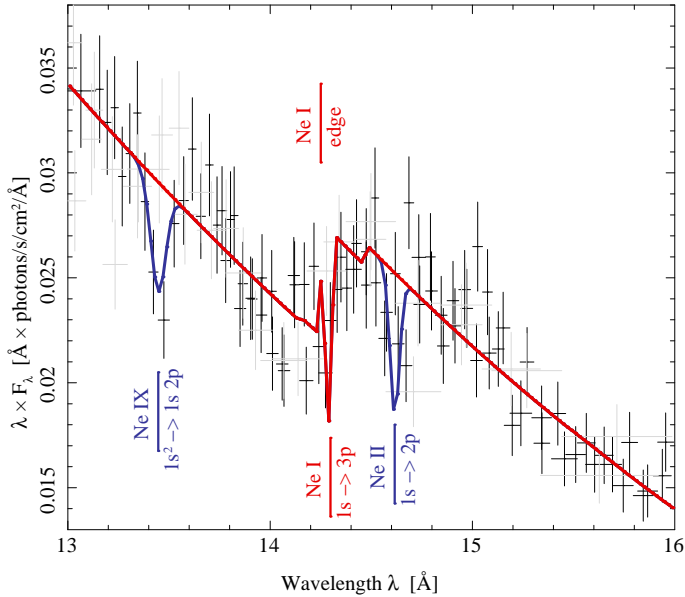


Fig. 4. The Ne-edge in observation X2. The first order RGS spectra (black) reveal absorption lines of Ne IX at 13.45 Å and probably also Ne II at 13.62 Å, but the quality of the spectrum does not allow for a detailed study of the ionized absorber.

Finally, we find marginal evidence for ionized absorption in the high-resolution spectra (Fig. 4), however, a detailed study of these features is beyond the scope of this paper.

4. Summary and Discussion

The elements with the largest contribution to the photoabsorption in the soft X-ray band are significantly less abundant in the LMC than in the Galaxy (Table 2). Because of the lower metallicity, simply using radio-measured N_{H} values in an absorption model without adopting the LMC abundances will not allow for a correct description of the physical situation. Specifically for LMC X-1, the *equivalent* hydrogen column density inferred from this X-ray absorption study – taking the proper LMC abundances into account – is actually much higher than the H-column resolved by the LAB survey (at a half-power beam-width of 0°6; Kalberla et al., 2005), which is likely due to additional material in the environment of LMC X-1 and in the system itself. This result was not obtained in earlier X-ray absorption measurements, as erroneously applying Galactic abundances resulted in smaller N_{H} values.

In addition, we have presented the first evidence that the column density varies in the range $(1.0\text{--}1.3)\times 10^{22}\text{ cm}^{-2}$. A modulation with orbital phase is strongly suggested and would be consistent with absorption in the stellar wind of the donor giant. Orosz et al. (2009) assume that the orbital modulation of the X-ray flux is mostly caused by Thomson scattering in the stellar wind as they find similar amplitudes⁶ in all the three *RXTE*-ASM energy bands, namely $A_{\text{A}(1.5\text{--}3\text{ keV})} = 7.2\pm 1.0\%$, $A_{\text{B}(3\text{--}5\text{ keV})} = 7.7\pm 1.1\%$, and $A_{\text{C}(5\text{--}12\text{ keV})} = 3.8\pm 2.9\%$. From a modulation in N_{H} with a full amplitude of $3 \times 10^{21}\text{ cm}^{-2}$, $A_{\text{A}} = 7.7\text{--}6.9\%$, $A_{\text{B}} = 1.6\text{--}2.7\%$, and $A_{\text{C}} = 0.4\text{--}1.7\%$ are expected, depending on the assumptions about the ASM response – i.e., the variation seen with the ASM is almost consistent with the

suggested neutral absorption. The phase of the current sine fit, however, is not. Further soft X-ray observations covering more phases are clearly needed, as the structure of the stellar wind might be more complex than a sine curve. With three 50 ks *Chandra* observations that we have gained for AO 11, we will be able to better constrain the modulation.

Acknowledgements. We thank N. Przybilla and M.F. Nieva for providing the LMC abundances. M.H. and J.W. acknowledge funding from the *Bundesministerium für Wirtschaft und Technologie* through the *Deutsches Zentrum für Luft- und Raumfahrt* under contract 50OR0701. We thank the MIT Kavli Institute and the ISSI (Bern) for their hospitality during the preparation of this work.

References

- Bajaja E., Arnal E.M., Larrarte J.J., et al., 2005, *A&A* 440, 767
 Burrows D.N., Hill J.E., Nousek J.A., et al., 2005, *SSR* 120, 165
 Canizares C.R., Davis J.E., Dewey D., et al., 2005, *PASP* 117, 1144
 Coppi P.S., 2000, *BAAS*, 32, 1217
 Cowley A.P., Hutchings J.B., Crampton D., 1978, *AJ* 83, 1619
 Cowley A.P., Schmidtke P.C., Anderson A.L., McGrath T.K., 1995, *PASP* 107, 145
 Cui W., Feng Y.X., Zhang S.N., et al., 2002, *ApJ* 576, 357
 den Herder J.W., Brinkman A.C., Kahn S.M., et al., 2001, *A&A* 365, L7
 Done C., Życki P.T., Smith D.A., 2002, *MNRAS* 331, 453
 Dufour R.J., 1984, In: van den Bergh S., Boer K.S.D. (eds.) *Structure and Evolution of the Magellanic Clouds*, IAU Symp. 108, p.353
 Ebisawa K., Mitsuda K., Inoue H., 1989, *PASJ* 41, 519
 Garnett D.R., 1999, In: Chu Y.H., Suntzeff N., Hesser J., Bohlender D. (eds.) *New Views of the Magellanic Clouds*, IAU Symp. 190, p.266
 Gierliński M., Maciołek-Niedźwiecki A., Ebisawa K., 2001, *MNRAS* 325, 1253
 Gou L., McClintock J.E., Liu J., et al., 2009, *ApJ* 701, 1076
 Haardt F., Galli M.R., Treves A., et al., 2001, *ApJS* 133, 187
 Houck J.C., Denicola L.A., 2000, In: Manset N., Veillet C., Crabtree D. (eds.) *Astronomical Data Analysis Software and Systems IX*. ASP Conf. Ser., 216, p.591
 Hutchings J.B., Crampton D., Cowley A.P., 1983, *ApJ* 275, L43
 Hutchings J.B., Crampton D., Cowley A.P., et al., 1987, *AJ* 94, 340
 Jansen F., Lumb D., Altieri B., et al., 2001, *A&A* 365, L1
 Kalberla P.M.W., Burton W.B., Hartmann D., et al., 2005, *A&A* 440, 775
 Korn A.J., Keller S.C., Kaufer A., et al., 2002, *A&A* 385, 143
 Korn A.J., Nieva M.F., Daflon S., Cunha K., 2005, *ApJ* 633, 899
 Levine A.M., Corbet R., 2006, *ATel*, 940
 Li L.X., Zimmerman E.R., Narayan R., McClintock J.E., 2005, *ApJS* 157, 335
 Mark H., Price R., Rodrigues R., et al., 1969, *ApJ* 155, L143
 Negueruela I., Coe M.J., 2002, *A&A* 385, 517
 Noble M.S., Houck J.C., Davis J.E., et al., 2006, In: Gabriel C., Arviset C., Ponz D., Enrique S. (eds.) *Astronomical Data Analysis Software and Systems XV*, ASP Conf. Ser., 351, p.481
 Noble M.S., Nowak M.A., 2008, *PASP* 120, 821
 Nowak M.A., Wilms J., Heindl W.A., et al., 2001, *MNRAS* 320, 316
 Orosz J.A., Steeghs D., McClintock J.E., et al., 2009, *ApJ* 697, 573
 Pakull M., 1980, *IAU Circ.* 3472, 1
 Price R.E., Groves D.J., Rodrigues R.M., et al., 1971, *ApJ* 168, L7
 Przybilla N., Nieva M.F., Heber U., et al., 2008, *A&A* 480, L37
 Richter O.G., Tammann G.A., Huchtmeier W.K., 1987, *A&A* 171, 33
 Schlegel E.M., Marshall F.E., Mushotzky R.F., et al., 1994, *ApJ* 422, 243
 Shrader C., Titarchuk L., 1998, *ApJ* 499, L31
 Smith D.M., Dawson D.M., Swank J.H., 2007, *ApJ* 669, 1138
 Steiner J.F., Narayan R., McClintock J.E., Ebisawa K., 2009, *PASP* 121, 1279
 Strüder L., Briel U., Dennerl K., et al., 2001, *A&A* 365, L18
 Suchy S., Pottschmidt K., Wilms J., et al., 2008, *ApJ* 675, 1487
 Titarchuk L., 1994, *ApJ* 434, 570
 Turner M.J.L., Abbey A., Arnaud M., et al., 2001, *A&A* 365, L27
 Wilms J., Allen A., McCray R., 2000, *ApJ* 542, 914
 Wilms J., Nowak M.A., Pottschmidt K., et al., 2001, *MNRAS* 320, 327
 Wilms J., Nowak M.A., Pottschmidt K., et al., 2006, *A&A* 447, 245
 Wilms J., Nowak M.A., Pottschmidt K., et al., 2003, In: Durouchoux P., Fuchs Y., Rodriguez J. (eds.) *New Views on Microquasars*, p.49
 Yao Y., Wang Q.D., Nan Zhang S., 2005, *MNRAS* 362, 229

⁶ The fractional full amplitude is here $A = (\text{max} - \text{min}) / \text{mean}$.